Journal of the Geological Society, London, Vol. **165**, 2008, pp. 1059–1073. Printed in Great Britain.

Timing and nature of Quaternary fluvial incision in the Ouarzazate foreland basin, Morocco

MARIA-LUISA ARBOLEYA[1], JULIEN BABAULT[1], LEWIS A. OWEN[2], ANTONIO TEIXELL[1] & ROBERT C. FINKEL[3]

[1]*Departament de Geologia, Universitat Autònoma de Barcelona, E-08193, Bellaterra, Spain (e-mail: MariaLuisa.Arboleya@uab.es)*

[2]*Department of Geology, University of Cincinnati, Cincinnati, OH 45221, USA*

[3]*Center for Accelerator Mass Spectrometry, Lawrence Livermore National Laboratory, Livermore, CA 92521, USA*

Abstract: The history of alluvial fan and terrace formation within a stretch of the Ouarzazate basin along the southern margin of the Central High Atlas is reconstructed using geomorphological and ^{10}Be terrestrial cosmogenic nuclide (TCN) methods. Alluvial fan and terrace incision was controlled partially by a drop in base level during the Pliocene or early Pleistocene as the outlet channel, the Draa river, progressively cut through the Anti-Atlas to the south of the Ouarzazate foreland basin, the drainage of which started to become external after a long period of internal drained conditions. The alluvial fans and terrace surfaces have abandonment ages that date to at least the past four glacial cycles. Their formation was strongly modulated by climate on glacial–interglacial time scales as base level dropped. This demonstrates a strong climatic control on sediment transfer and landscape denudation during the Quaternary and provides a model for understanding sediment transfer in other intracontinental mountain belts. Furthermore, these data show that mean rates of fluvial incision in this region range between 0.3 and 1.0 mm a^{-1} for the latter part of the Quaternary. This study provides the first comprehensive TCN chronology for the Atlas Mountains, and it illustrates the applicability and limitations of TCN methods.

Understanding the nature of denudation, sediment transfer and deposition, and landscape evolution in foreland basins is important for defining and quantifying tectonic and geomorphological models for orogenesis. Numerous studies have shown that sedimentation during foreland basin development may progressively advance away from the mountain belt as deformation propagates into the foreland and as proximal basins overfill with sediment (Flemings & Jordan 1989; Sinclair *et al*. 1991; DeCelles & Giles 1996). These studies have broadly defined the rates of sedimentary and geomorphological processes on million year time scales, generally spanning the Cenozoic and/or Mesozoic. There are few studies, however, that provide data on millennial time scales that span the Quaternary. Given the high frequency and the large magnitudes of climatic change throughout the Quaternary, it is likely that there has been a strong climatic control on geomorphological and sedimentary processes in general during this time span and that these climatic controls have ultimately controlled the nature of the landscape evolution of foreland basins. We therefore undertook a study of the Ouarzazate basin in Morocco to examine the nature of Quaternary landscape evolution of a foreland basin in the context of Quaternary climate change.

The Ouarzazate basin is sandwiched between the High Atlas and the Anti-Atlas Mountains to the north and south, respectively (Fig. 1). The Atlas mountain system is considered as a type example of an intracontinental mountain belt (Mattauer *et al*. 1977; Rodgers 1987; Ziegler *et al*. 1995). This active mountain system formed during the Cenozoic in the interior of the African plate ahead of the Rif–Tell plate boundary orogen.

Impressive alluvial fans and terraces rising more than 100 m above active rivers flowing from the High Atlas are present within the Ouarzazate basin. These fans and terraces record a history of sedimentation and denudation that allows rates of denudation to be determined. Using geomorphological mapping, sedimentology, and the ^{10}Be terrestrial cosmogenic radionuclide (TCN) method, the recent history of sedimentation and erosion within a stretch of the Ouarzazate basin was reconstructed to provide one of the first studies of the geomorphological evolution of an intracontinental mountain belt foreland basin that is defined by Quaternary geochronology, representing one of the first chronological datasets for continental NW Africa.

Significant work has been undertaken on alluvial fans and terraces around the Mediterranean, notably by Harvey & Wells (1987), Macklin *et al*. (1995, 2002), Fuller *et al*. (1998), Rose *et al*. (1999), Kelly *et al*. (2000), Mather (2000), Santisteban & Schulte (2007) and Schulte *et al*. (2008). These studies argue for strong links between climate, the fluvial system and landscape evolution. However, no studies of the geomorphology of alluvial fan and terraces have been undertaken in the forelands of the Atlas Mountains. Our paper therefore presents the first quantitative chronologies on terraces for the region, which begin to test key questions about the role of tectonics, climate and autocyclicity in landscape evolution in the Atlas Mountains and adjacent regions.

Research area

The Ouarzazate basin is situated within the Alpine foreland of the Rif–Tell orogen, which comprises several intracontinental mountain belts and plateaux. The Atlas chains developed as a consequence of continental convergence between Africa and Europe, from the inversion of Jurassic rift or transtensional basins during the Cenozoic (Choubert & Faure-Muret 1962; Mattauer *et al*. 1977; Schaer 1987; Jacobshagen 1988; Laville &

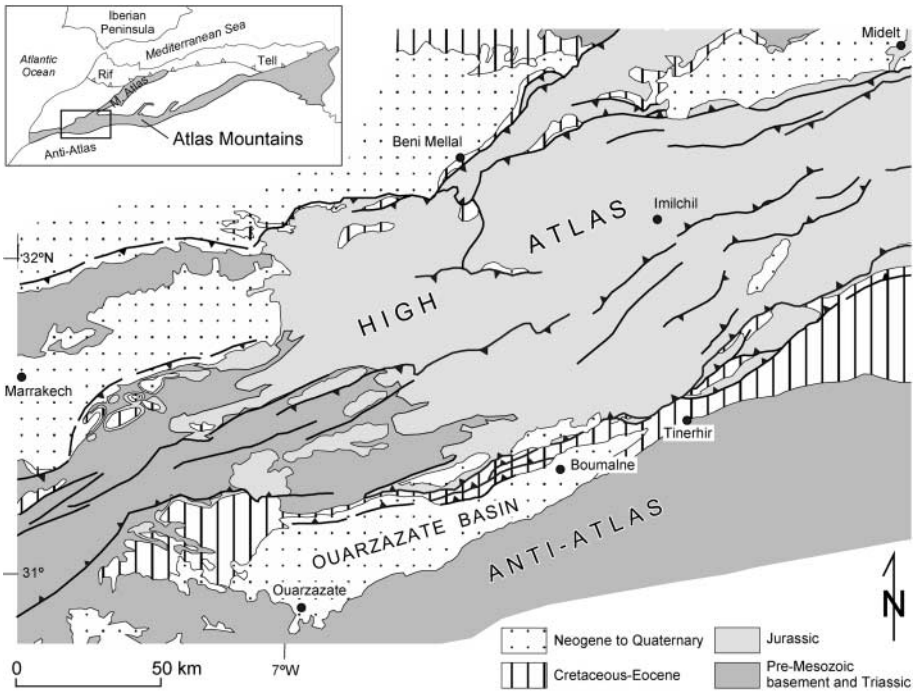

Fig. 1. Simplified geological map of the western part of the Central High Atlas Mountains, the Ouarzazate basin, and the Anti-Atlas Mountains. Inset shows the location of the map region in the Atlas mountain system of NW Africa.

Piqué 1992; Beauchamp *et al*. 1996; Frizon de Lamotte *et al*. 2000; Gomez *et al*. 2000; Teixell *et al*. 2003; Arboleya *et al*. 2004). The High Atlas forms the most prominent mountain chain, rising to 4000 m above sea level (a.s.l.); it is *c*. 100 km wide, and extends roughly east–west for 2000 km from Morocco into Algeria and Tunisia (Fig. 1, inset), where the range is known as the Saharan Atlas and the Tunisian Atlas, respectively. The High Atlas is composed at the surface of deformed Precambrian, Palaeozoic and Mesozoic rocks (mostly Jurassic) (Fig. 1). Flanking the High Atlas to the south, the Anti-Atlas Precambrian–Palaeozoic massif is a zone of wide domal uplift with much weaker Alpine deformation, but still reaches altitudes of more than 2000 m a.s.l. Part of the highly elevated topography of the Atlas system is due to crustal shortening and thickening, but a fraction of it is related to mantle upwelling (Teixell *et al*. 2003; Ayarza *et al*. 2005), expressed by 100 km scale lithospheric thinning (Teixell *et al*. 2005; Zeyen *et al*. 2005; Missenard *et al*. 2006).

The Ouarzazate basin is located between the High Atlas and Anti-Atlas Mountains; it has an elevation of 1200–1800 m a.s.l., extends more than 150 km roughly east–west and reaches a width of 40 km near its western end (Fig. 2a). The basin is filled with a thin (<1 km) succession of Cenozoic molasse that comprises alluvial, fluvial and lacustrine sediments (Fraissinet *et al*. 1988; Görler *et al*. 1988; El Harfi *et al*. 2001; Tesón & Teixell 2008). The Cenozoic sediments onlap the Precambrian to Palaeozoic rocks of the Anti-Atlas to the south and are overthrust by the High Atlas to the north (Fig. 2b). Basin rocks of Tertiary age are deformed by a series of southward verging folds and blind thrusts that propagate from the High Atlas Mountains (Fig. 2b). The Quaternary deposits are less deformed (Couvreur 1973; Sébrier *et al*. 2006) and comprise essentially fanglomerates, which radiate southward and cap the older rocks (Fig. 2a).

Streams drain southward and northward into the Ouarzazate basin from the High Atlas and Anti-Atlas Mountains, respectively. Most of these are ephemeral and experience flash floods during heavy rainstorm events. These ephemeral streams ultimately drain into the Draa river (Fig. 2a), which was perennial until the recent construction of a dam south of Ouarzazate. The Draa river traverses the Anti-Atlas and has cut a deep box-shaped gorge, which is >300 m deep (Figs 2b and 3). Impressive successions of terraces are present along the streams that drain the High Atlas Mountains. These terraces comprise straths in Cenozoic rocks and are capped with Quaternary fanglomerates. At least six well-defined surfaces comprising alluvial fans, terraces and an active stream (Q1–Q6) can be recognized along most of the main drainages. These are well illustrated in the Madri and Izerki valleys (Figs 2a, 4 and 5). The Madri river drains the High Atlas, in an area where the rocks that crop out are mostly Precambrian to Palaeozoic in age, consisting primarily of slate, greywacke and rhyolite. The mountainous headwaters of the Madri river drains an area of *c*. 66 km^2 before joining its main tributary, the Tagragra river, located to the west (Fig. 2), which drains an area of *c*. 84 km^2. The mean elevation of the entire Madri–Tagragra catchment is 2275 m a.s.l., and the fraction of the catchment lying above 3300 m a.s.l. is negligible (0.15%, i.e. *c*. 0.2 km^2). The Madri basin, therefore, lies below the snowline (3300 m a.s.l.) for the coldest stages of the Pleistocene (Dresch 1941; see also references given by Hughes *et al*. 2004, 2006).

The climate of the Ouarzazate basin is sub-Saharan, situated within the subtopical high-pressure system. Precipitation ranges from 1 to 20 mm per month, with the heaviest rainfall occurring between December and March, and totals *c*. 100 mm a^{-1} (Knippertz *et al*. 2003). Temperature in the region ranges from 1 to 37 °C (Allmetsat 2007). Vegetation within the Ouarzazate basin is sparse, comprising small xerophytic shrubs.

Field methods

Field work was undertaken throughout the Ouarzazate basin. The Madri valley was chosen for detailed study because it contains some of the best-formed and most well-preserved terraces (Figs 4 and 5). Furthermore, the valley is one of the major drainage

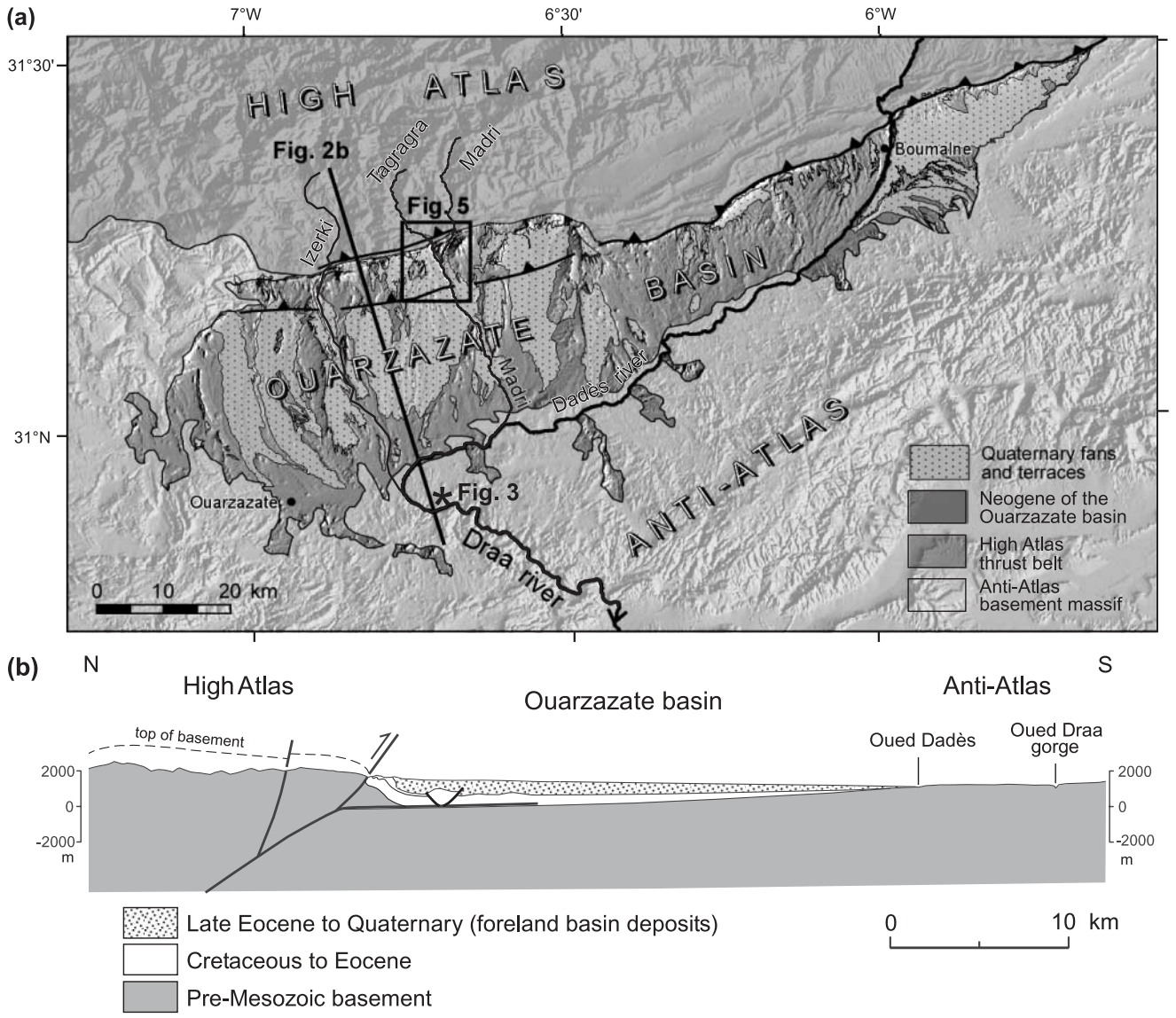

Fig. 2. (**a**) Map of the distribution of Quaternary fans and terraces in the Ouarzazate basin. (**b**) Cross-section of the Ouarzazate basin located between the High Atlas and the Anti-Atlas Mountains. This shows the wedge geometry of the basin and the low thickness of sediments accumulated in it (<1000 m). Deformation in the High Atlas propagates to the south, leading to Neogene and Quaternary thrusts and folds within the basin.

systems along the southern margin of the High Atlas Mountains (Fig. 2a). In addition, the catchment area is composed mostly of rhyolite and other rocks that have high quartz contents, which is essential for ^{10}Be TCN surface exposure dating. A tectonically deformed terrace west of the Madri valley was also studied and dated to examine the possible effect of surface erosion during its deformation (Fig. 4c). An extensive surface that extends for about 15–20 km to the west of the Madri valley was also sampled at a location *c*. 11 km from the river (31.17°N, 6.80°W), where there was no evidence of surface deformation or erosion.

Geomorphological mapping aided by remote sensing using ASTER images (http://asterweb.jpl.nasa.gov/) and cross-valley profiles were used to determine the sizes and relative ages of the terraces and fan surfaces within the study areas (Figs 5 and 6). The terraces, alluvial fan and active channel surfaces were numbered Q1 (oldest) to Q6 (youngest). Sedimentary sections were studied at natural exposures to examine the terrace and fan deposits. Where fan surfaces were not contiguous, correlations were based on relative elevations and surface characteristics. These surface characteristics are listed in Table 1 and are shown in Figure 7.

The development of TCN methods in recent years has allowed alluvial fan surfaces in drylands to be successfully dated; studies using these methods include those by Zehfuss *et al*. (2001), Matmon *et al*. (2005), Benn *et al*. (2006), Akçar *et al*. (2007), Frankel *et al*. (2007*a*, *b*) and Le *et al*. (2007). We build on the methods used in these studies for sampling and interpretation of the age data.

Samples for TCN surface exposure dating were collected by chiselling off *c*. 500 g of rock from the upper surfaces of quartz-rich boulders on high areas of terrace surfaces. Locations were chosen where there was no apparent evidence of exhumation or slope instability. The largest boulders were chosen to help reduce the possibility that boulders were previously covered with

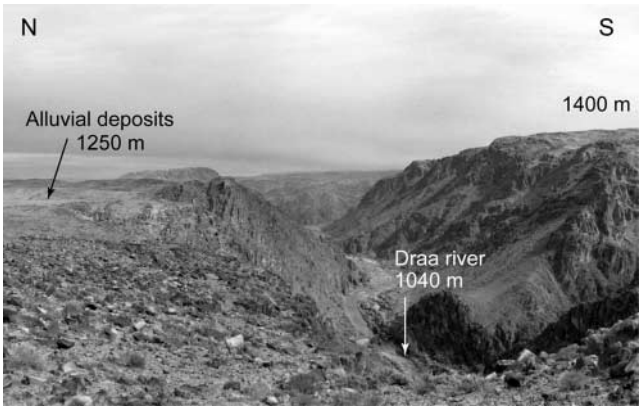

Fig. 3. The Draa canyon in the Anti-Atlas (location shown in Fig. 2a). South of the Ouarzazate basin margin, in the Anti-Atlas Precambrian rocks, the Draa river incision is more than 300 m deep. The view also shows light-coloured, flat-lying conglomerate deposits of Anti-Atlas origin resting on the crystalline basement (arrow). The aggradation of these Mio-Pliocene alluvial deposits near the ridge of the Anti-Atlas suggests that overfilling of the Ouarzazate basin is a possible cause for the change from internal to external drainage.

sediment. The typical boulder diameter was 70 cm; the dimensions of all sampled boulders are listed in Table 2. Several (four to seven) boulders were sampled from each alluvial fan or terrace surface (Q1–Q5). Two boulders within the active stream surface (Q6, boulders Maroc-50 and 51) were also collected. The degree of weathering and the site conditions for each boulder were recorded. In all cases, no topographic shielding correction was necessary.

Laboratory methods

All the samples for TCN surface exposure dating were prepared in the geochronology laboratories at the University of Cincinnati. First, the samples were crushed and sieved. Quartz was separated from the 250–500 μm fractions using the methods of Kohl & Nishiizumi (1992). After addition of ^{9}Be carrier, Be was separated and purified by ion exchange chromatography and precipitated at pH >7. Be-bearing hydroxides were oxidized by ignition in quartz crucibles. BeO was then mixed with Nb metal and loaded onto targets for the determination of ^{10}Be/^{9}Be ratios by accelerator mass spectrometry (AMS) at the Center for Accelerator Mass Spectrometry at the Lawrence Livermore National Laboratory (USA). Isotope ratios were compared with ICN Pharmaceutical Incorporated ^{10}Be and NIST (National Institute Standard of Technology) standards prepared by K. Nishiizumi (pers. comm.) and using a ^{10}Be half-life of 1.35×10^{6} years. The measured isotope ratios were converted to TCN concentrations in quartz using the total ^{10}Be in the samples and the sample weights. TCN ^{10}Be concentrations were then converted to zero-erosion exposure ages using a sea-level high-latitude (SLHL) ^{10}Be production rate of 4.98 atoms g^{-1} of quartz per year (Stone 2000). There is currently much debate regarding the appropriate scaling models and geomagnetic corrections for TCN production to calculate surface exposure ages (e.g. Pigati & Lifton 2004; Staiger *et al*. 2007; Balco *et al*. 2008). We chose to use ^{10}Be production rates scaled to the latitude and elevation of the sampling sites, applying the time-independent scaling factors of Lal (1991) and Stone (2000) with 3% SLHL muon contribution, using the CRONUS Earth 2 calculator (Balco *et al*. 2008; http://hess.ess.washington.edu/math/). However, we recognize that other scaling models would produce ages that may differ by up to 20% (see Balco *et al*. 2008). We also calculated the TCN ages for an erosion rate of 3 m Ma^{-1}, which we believe is the maximum possible erosion in this environment (see discussion below). Several sample ages (the oldest samples) could not be calculated for 3 m Ma^{-1} erosion because they were incompatible with this erosion rate.

Age determination methods: accuracy and limits

Several problems are commonly recognized with TCN surface exposure dating and it is important to discuss these before assigning ages to each terrace. The first is that sampled boulders may retain a signal of prior exposure inherited from their previous location, sometimes referred to as 'derived' boulders (Anderson *et al*. 1996; Hancock *et al*. 1999). Collecting multiple samples from each terrace and looking for potential outliers, that is, exposure ages that fall significantly outside (>2σ) the weighted mean value for all the ages obtained for a given landform, can help us to recognize the potential problem of derived boulders. Furthermore, a second check on prior exposure can be made by dating boulders from the modern floodplain (Anderson *et al*. 1996). Young ages from the floodplain suggest little inheritance whereas old ages highlight a potential inheritance problem. A second problem is that boulders can produce erroneously young TCN surface exposure ages. This is usually caused by boulders that have been exhumed or toppled. The potential of exhumation can be reduced by choosing the largest boulders on a surface, sampling on ridges (not depressions) on a landform surface, choosing boulders with maximum relief above the surface (Table 2), and sampling the highest point on each boulder surface. The potential for sampling toppled boulders is reduced by choosing boulders on the distal edges of a landform to avoid toppling from higher surfaces and by sampling boulders that appear well embedded in the landform surface.

Disregarding problems of inheritance, TCN concentrations can be interpreted as either minimum exposure ages (assuming zero erosion) or maximum erosion rates (erosional equilibrium). For estimating steady-state erosion rates, samples with older apparent exposure ages provide limits on erosion rates. For many of the samples collected in the study area, maximum erosion rates of 1–3 m Ma^{-1} were calculated using the oldest boulders by applying the methods of Lal (1991). Given that these are maximum erosion rates and that it is unlikely that they are in erosional equilibrium because the preserved fluvial forms (rounded smooth surfaces) on many of the boulders suggest moderate to little erosion, a reasonable estimation of erosion for boulders in the study area is *c*. 1 m Ma^{-1}. Furthermore, the absence of notable weathering features, such as exfoliated surfaces, suggests that erosion of boulders is <1 m Ma^{-1}. Assuming that all boulders weather at this rate, we can assess the impact of this amount of erosion on our chronologies. For samples having a 1 m Ma^{-1} erosion rate, an age of 10 ka would increase uncertainty by 1%; an age of 50 ka, by 4%; an age of 100 ka, by 10%; an age of 200 ka, by 22%; and an age of 300 ka, by 42%. An erosion rate of 1 m Ma^{-1} is consistent with the TCN data from studies in other dryland regions (Small *et al*. 1997; Zehfuss *et al*. 2001; Owen *et al*. 2006). Given the uncertainties in defining the erosion rate, we plot all our data with zero erosion, but also present the ages in Table 2 for an erosion rate of 3 m Ma^{-1}, which places an upper limit on the possible ages when considering erosion in this region.

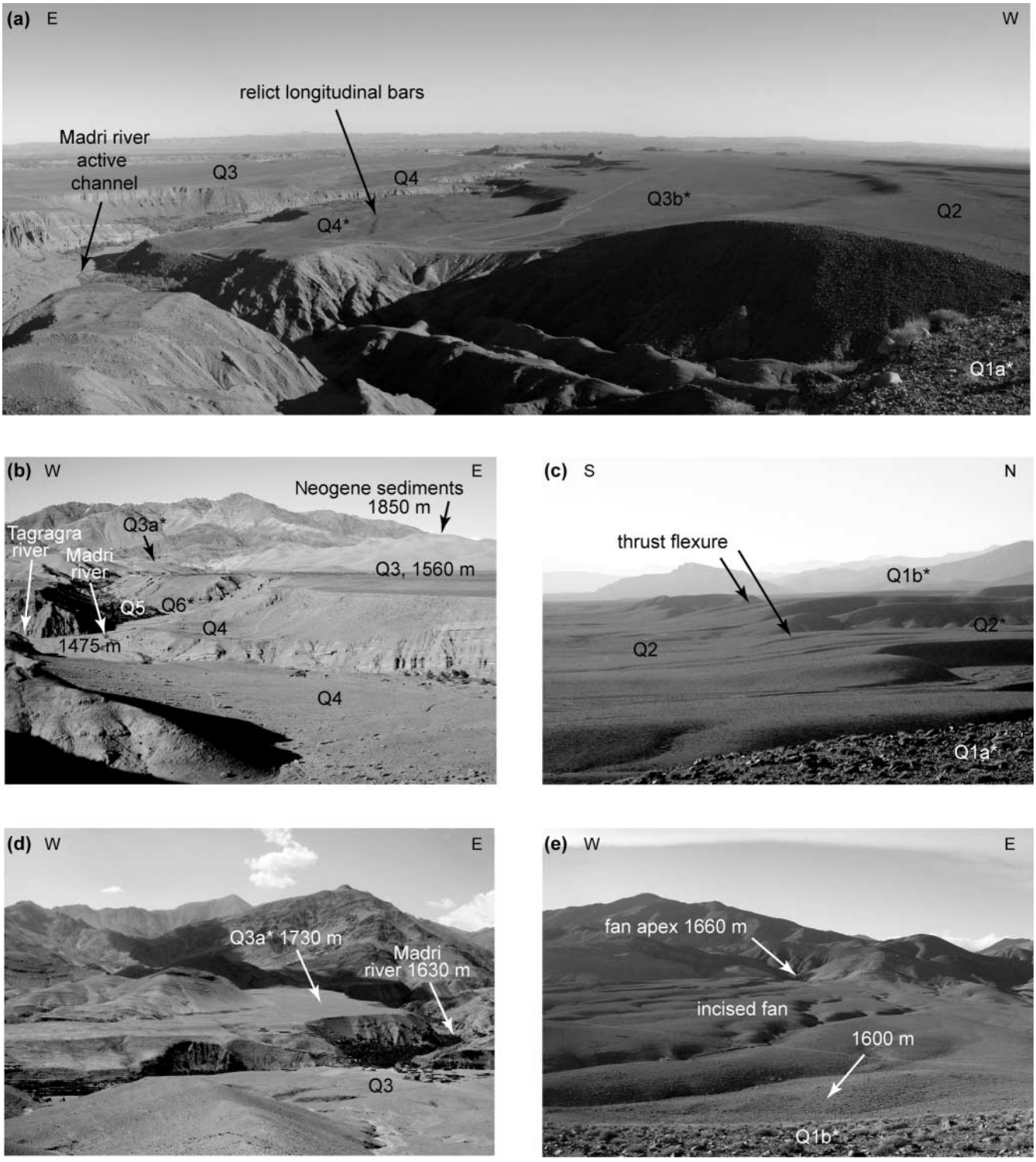

Fig. 4. Succession of terraces in the Madri (**a**, **b** and **d**) and Tagragra (**c** and **e**) valleys (terrace locations shown in Fig. 5) The asterisks indicate the sampled terraces. (**a**) Madri river viewed to the south towards the Anti-Atlas (ridge line in the background). Terraces Q2 and Q3 are very extensive and merge to the south of the study area. Longitudinal bars are preserved on terrace Q4. In the foreground, the badlands are Neogene deposits tilted to the south and cut by the strath terraces. (**b**) Madri river viewed northwards towards the High Atlas showing four fill-terraces (Q3–Q6). Terraces Q2 to Q5 lie at elevations ranging from 1585 m to 1510 m a.s.l., respectively (see topographic profile 2, Fig. 6). In the background the sampled terrace Q3a reaches an elevation of 1740 m a.s.l. (see topographic profile 3, Fig. 6). The terraces are inset into the Neogene basin fill, which reaches an elevation of around 1850 m a.s.l. on the northern border of the Ouarzazate basin. (**c**) Folding is active in this part of the Ouarzazate basin: in the area shown, flexure of terrace Q2 generated an offset of 20 m. (**d**) Abandoned and deeply incised fan Q3a viewed to the north near the High Atlas Mountains front. (**e**) Poorly incised fan located west of the Tagragra river viewed to the north; distance from the foreground to the fan apex is 1500 m. Foreground is the sampled surface Q1b.

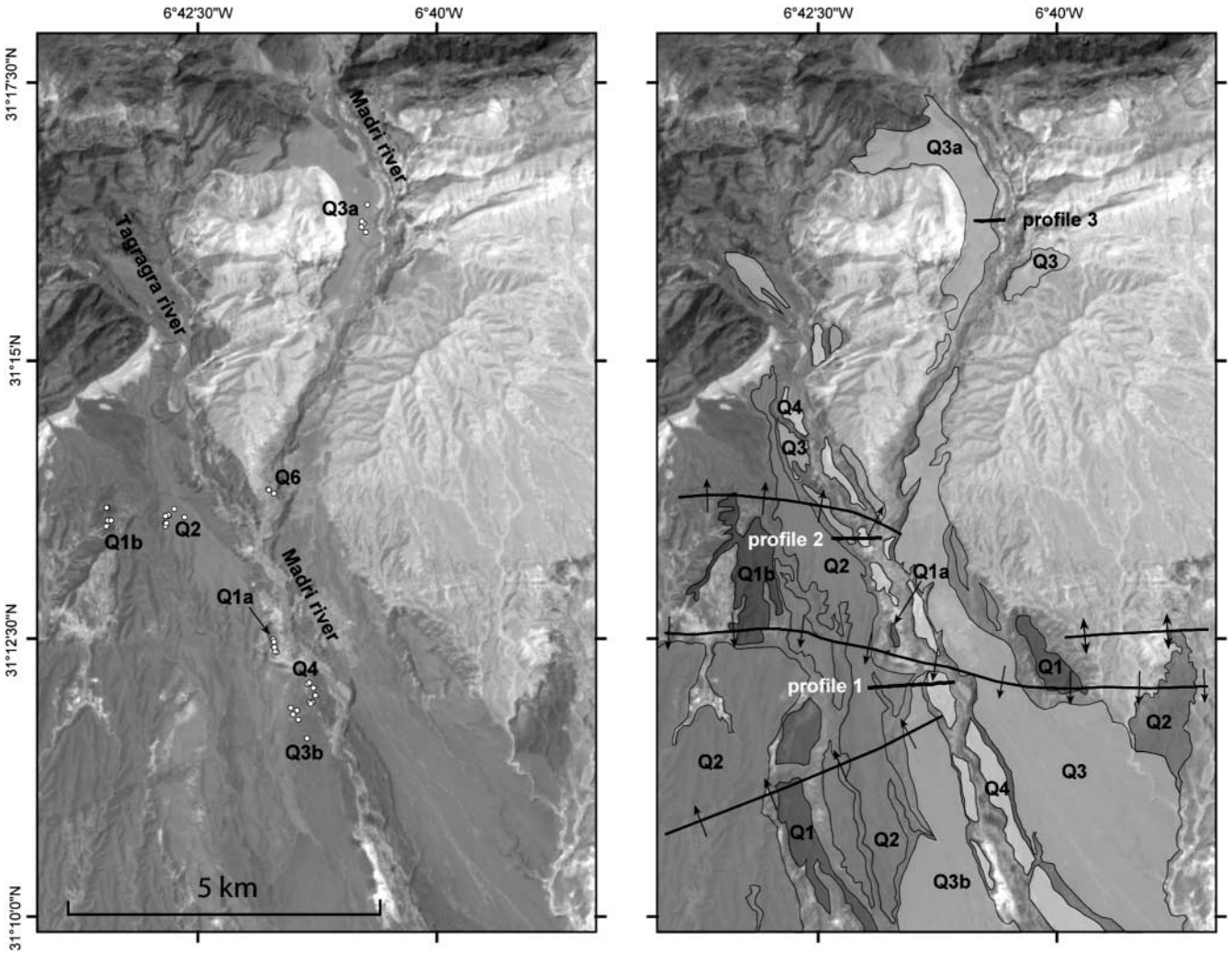

Fig. 5. ASTER image of the study area showing the location of samples (left) and the mapped terraces (right). Also shown are the flexure and folding axes of the Neogene and Quaternary deposits. Sample Q3c is not shown in this figure but is located *c*. 10 km to the west of the mapped area (Table 2 provides detailed locations). The trend of the Amekchoud anticline is highlighted in the right hand panel by the black line and dip arrows.

Results

The geomorphology of the terraces within the study area is illustrated in Figures 4–6. The terraces are more incised near the mountain front, where the sedimentary deposits are thickest (see terrace Q3a in Fig. 4d and inset in Fig. 6). The thickness of the Quaternary sediments varies considerably along the length of each valley, reflecting infilling of large channels many tens of metres across and more than 10 m deep. The sediments comprise well-rounded clast-supported cobbles and metre-size boulders in a sandy matrix, and show crude downvalley, low-angle cross-stratification. Over most of the length of each terrace the capping Quaternary sediments are 3–5 m thick.

Given the caveats discussed in the previous section, we assign modelled ages to each of the dated surfaces. These modelled ages represent the time when the terrace surface was abandoned, leaving the boulders exposed to cosmic rays. Tables 1 and 2 list the results of the TCN surface exposure dating, and in Figure 8 these data are plotted as scatter graphs and probability distributions. The range of ages for each surface varies considerably (third column in Table 1). This probably reflects the variability of geomorphological processes on terrace surfaces as discussed above and the range is greatest for the oldest surfaces. However, for many of the surfaces there is a clustering of ages (fourth column in Table 1), notably Q3 and Q4 surfaces. Given the clustering of ages and identification of possible inherited, exhumed, toppled and weathered boulders, an age is assigned to each surface (fifth column in Table 1). Table 2 also provides details on the lithology and size of the boulders dated and their weathering characteristics. The more resistant lithologies, and larger and less weathered boulders would be expected to give the oldest age on any given surface. However, there is no clear relationship in the dataset between boulder size and/or weathering characteristic and the age of the boulder for a particular surface, so it is difficult to explain anomalously young ages as a direct consequence of weathering.

Surface Q6 is the active channel of the Madri river and two dated boulders in this channel give ages of 0.5 ka and 19 ka. The first sample indicates that there is almost no inheritance in the active channel and the second one indicates that there may be some inheritance in some boulders but this is probably not important given the very old ages for most terraces (see below).

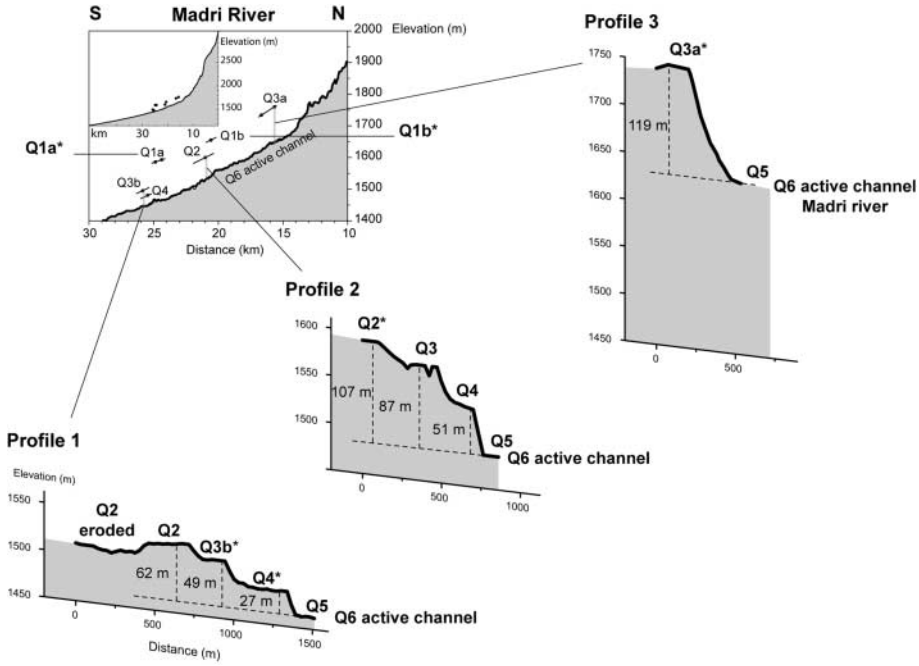

Fig. 6. Site location of abandoned filled terraces on transverse and longitudinal profiles. Along the Madri river, three transverse topographic profiles (numbered 1, 2 and 3 from downstream to upstream) have been performed where terraces have been sampled except for terraces Q1a, Q1b and Q2. Samples Q1a are located between profiles 1 and 2. Samples Q2 and Q1b are located 600 m NW and 1600 m west of profile 2, respectively (see Fig. 5). The asterisks indicate the sampled terraces. Graph in the upper left corner shows the sampled terraces projected (dots) onto the longitudinal profile of the Madri river extracted from SRTM90 DEM. Inset shows the longitudinal profile from the source to the confluence of the Madri river with the Dades river.

Surface Q5 is less than a few metres above the present channel. This terrace is used for agriculture and sampling was not possible, although it is likely that surface Q5 is historical.

Surface Q4 has ages that range from 7 to 36 ka, but the ages cluster between 7 and 11 ka. The pristine nature of the surface (well-preserved bar and swale forms and imbricated boulders) support the view that boulders Maroc-20 (36 ka) and Maroc-21 (23 ka) have inherited TCN. Therefore it is likely that this surface formed during the early Holocene or at the end of the Late-glacial.

Surface Q3 is very extensive in the southern part of the Ouarzazate basin. This surface was dated at three locations, which are named Q3a, Q3b and Q3c (see Table 2 for sampling locations). Ages span 85–105 ka, 87–121 ka and 84–93 ka, and cluster at 85–95 ka, 87–100 ka and 84–93 ka, respectively. An age range of 87–93 ka is favoured given that the surfaces are contemporaneous. Given some weathering (1 m Ma^{-1}), these ages become *c*. 10% older (*c*. 96–102 ka) and a maximum value of 3 m Ma^{-1} yields ages of 113–125 ka. The abandonment age for the Q3 surface corresponds broadly to marine oxygen isotope stage 5c. The age of the Q3 surface could straddle marine isotope stage 5e, however, given the uncertainty associated with the different scaling models and geomagnetic corrections that may be applied to calculate TCN ages (see discussion above). We favour the view that incision and abandonment of the sediments that form the Q3 surface occurred during the wetter last interglacial, but recognize the possibility that the surface may have formed during marine isotope stage 5c or earlier.

Surface Q2 is an extensive surface that can be traced in the upstream parts of the Ouarzazate basin. Near our sampling location, this surface has been gently deformed into a 2 m high broad flexure, as a result of the foreland propagation of thrust faulting. The ages on this surface range between 129 and 295 ka, but cluster between 163 and 174 ka. Samples Maroc-16 (129 ka) and Maroc-15 (295 ka) are probably from weathered–exhumed and derived boulders, respectively. Given a weathering rate of 1 m Ma^{-1}, the remaining ages should be *c*. 22% older (*c*. 196–211 ka), which suggests terrace deposition during the penultimate interglacial (marine oxygen isotope stage 7e) with incision and abandonment during post- or late-penultimate interglacial time.

The oldest surface, Q1, occurs on the top of mesas within several kilometres of the mountain front throughout the basin. These mesas have been deformed (Fig. 4c) and are intensely eroded. To test the stability of deformed surfaces, samples were collected from two relicts of the deformed surface Q1: the first along the Madri river (Q1a) and the second several kilometres west of the Tagragra river (Q1b). Both sample sites are between two flexures that merge to the east into the flanks of the east–west-trending Amekchoud anticline (Fig. 5).

Ages on surface Q1a range from 7 to 214 ka, but cluster around 193–214 ka. This wide range of ages probably reflects strong erosion, particularly for sample Maroc-8 (7 ka), which probably was recently exhumed. Given the 1 m Ma^{-1} erosion rate, the ages on this surface are likely to be at least 30% older and fall in the range 250–278 ka. The oldest boulder is most probably closest to the true age of the surface given that the surface has been eroded. Therefore surface Q1 is older than marine isotope stage 7e. Given the glacial–interglacial temporal spacing of the other terraces and the strong carbonate development (stage IV–V of Gile *et al*. 1981) in the terrace sediments for Q1, we assign Q1 to the interglacial of marine oxygen isotope stage 9c. However, this is tentative as the ages are widely scattered, probably because the surface has been deformed and eroded.

North of the Q1a area, surface Q1b is deformed into a steep monocline that rises between 5 and 7 m. This represents a ramping thrust that is related to foreland-propagating deformation from the High Atlas. Although this surface morphostratigraphically correlates with Q1a, the boulder ages range from 94 to 131 ka and they cluster between 109 and 124 ka. These are significantly younger ages compared with those of surface Q1a, and suggest that the Q1b surface has experienced considerable erosion.

Rates of fluvial incision (determined by dividing the elevation between surfaces by their ages) can be estimated using the depth of incision of terraces Q2–Q4 from profiles measured in the field

Table 1. *Descriptions and TCN ages for terraces in the Madri valley and the adjacent region*

Surface name	Sample numbers	Age range using 0 m Ma^{-1} erosion (ka)	Age cluster using 0 m Ma^{-1} erosion (ka)	Favoured age (ka)	Surface altitude (m asl)	Description of surface
Q1a	Maroc-4, and 6 to 10	7–214	193–214	250–278; MIS-9c	1590	This is the highest surface and occurs on top of small mesas. It is present within several kilometres of the mountain front throughout the basin. The surfaces undulate and have well-developed desert pavements. Most surfaces may have experienced considerable deflation and erosion prior to desert pavement formation. The surface sediments have a well-developed carbonate cement (carbonate morphology stage IV–V of Gile *et al*. 1981)
Q1b	Maroc-35 to 38, 40 and 41	94–131	109–124	MIS-9c	1660	This surface has the same general characteristics as Q1, but it is warped, deformed by a growth fold. It has areas of pronounced erosion
Q2	Maroc-11, and 13 to 17	129–295	163–174	MIS-7e	1600	This surface is planar and can be traced for many tens of kilometres across the basin. It has a well-developed desert pavement, but few boulders larger than 1 m in diameter. In places this surface is subtly deformed by growth folds and faults. A 10–15 cm thick calcrete layer is present across part of this surface and the clasts within the first few metres of this surface are densely cemented with carbonate (carbonate morphology stage IV–V of Gile *et al*. 1981)
Q3a	Maroc-27, 29, 30, 31, 33 and 34	85–105	85–95	MIS-5e	1730	Apex of fan near Imin Tazarhgt village. Contains many boulders, with abundant bars and swale forms (carbonate morphology stage III of Gile *et al*. 1981)
Q3b	Maroc-42, 43, 46, 47 and 49	87–121	97–100	MIS-5e	1495	This is an extensive surface that can be traced many kilometres along and down the basin. The surface is a flat surface with occasional metre-size boulders. The surface is deformed by a growth fold. The upper 2 m of sediment has porous carbonate cement (carbonate morphology stage III of Gile *et al*. 1981)
Q3c	Maroc-112, 113, 115 to117	84–93	84–93	MIS-5e	1450	This is an extensive surface that can be traced for several tens of kilometres. The surface is very flat, but faulted and warped in place, and it has occasional metre-size boulders. The upper 2 m of sediment has porous carbonate cement (carbonate morphology stage III of Gile *et al*. 1981)
Q4	Maroc-20 to 26	7–36	7–11	Early Holocene	1482	Surface with many large boulders (>1 m in diameter). The boulders are commonly imbricated and form longitudinal bars. Desert pavement is present between these bars. Millimetre-thick carbonate rims are present around clasts within the top few metres of the surface sediment (carbonate morphology stage II of Gile *et al*. 1981)
Q5	Maroc-52	Not dated				Historical terrace; many boulders on agricultural terrace. No carbonate development
Q6	Maroc-50 and 51	0.5–19	Not applicable	recent	recent	Active channel; abundant large boulders. No carbonate development

MIS, marine oxygen isotope stage.

(Fig. 6) and the assigned ages. Assuming that incision and abandonment occurred during each interglacial, we use Winograd *et al*. (1997) interglacial termination ages for the interglacials that are assigned to the surfaces to provide maximum incision rates. Incision rates based on surface Q2 are 0.28 mm a^{-1} and 0.49 mm a^{-1} for profiles 1 and 2, respectively. For surface Q3, calculated incision rates are 0.39 mm a^{-1}, 0.70 mm a^{-1} and 0.95 mm a^{-1} for profiles 1, 2, and 3, respectively. If we assign the Q3 surface to marine isotope stage 5c, the incision ranges from 0.51 to 1.24 mm a^{-1}. The rates of incision for the Q4 surface are less than 2.45 mm a^{-1} and less than 5.18 mm a^{-1} for profiles 1 and 2, respectively. The higher incision rates for Q4 probably reflect the fact that the present interglacial cycle is not yet complete, and given more time the rates are likely to be

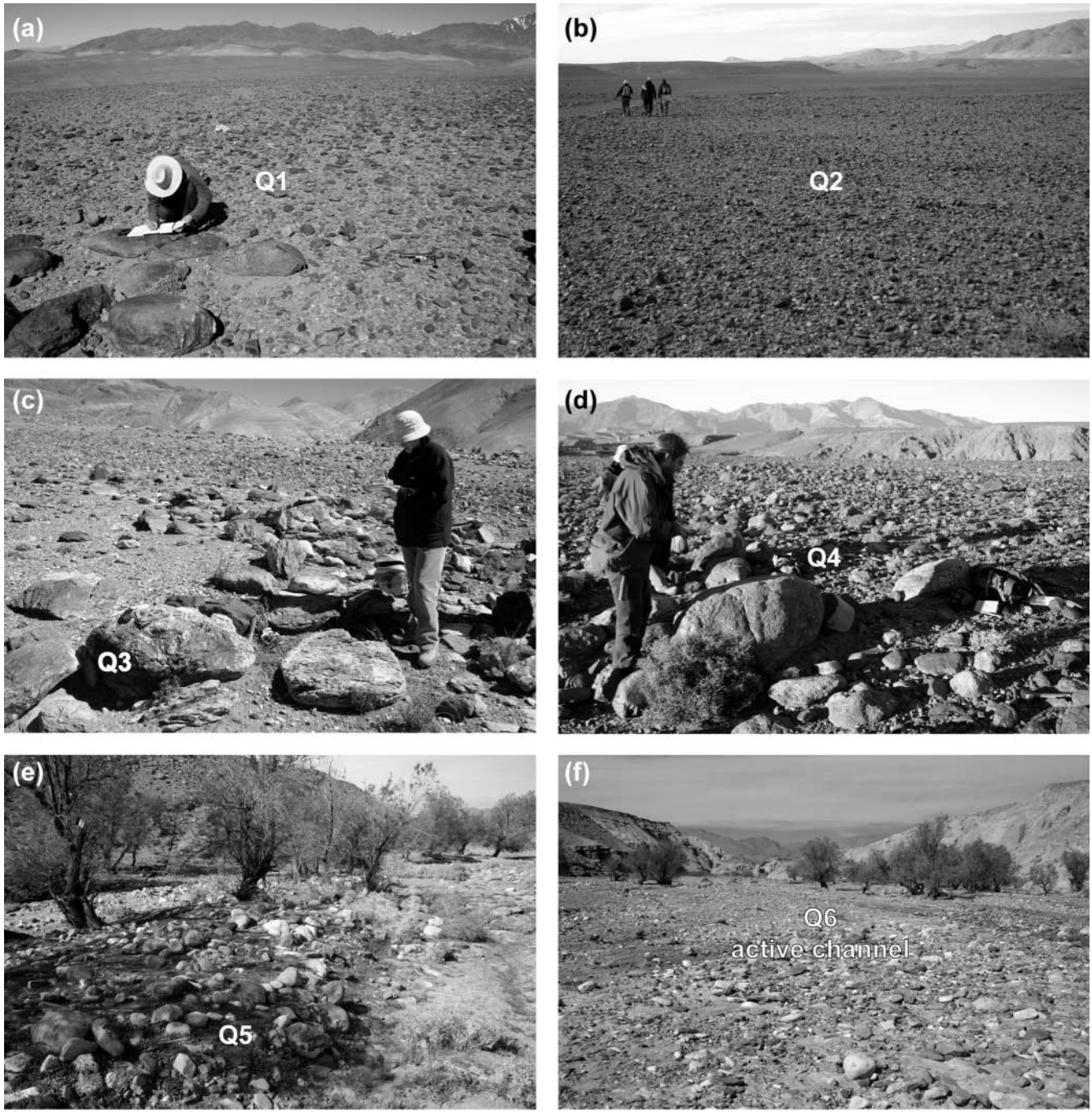

Fig. 7. Detail views of terrace surface characteristics. (**a**) Q1; (**b**) Q2; (**c**) Q3; (**d**) Q4; (**e**) Q5; (**f**) Q6. Terrace characteristics are described in Table 1.

substantially reduced. The fluvial incision rate calculations based on the terraces in our study area is in accordance with rates of fluvial incision for other semi-arid environments (e.g. Anders *et al*. 2005).

Discussion

The history of the Ouarzazate foreland basin can be broadly divided into two periods. Its early record is dominated by net sedimentation as Tertiary fluvial and lacustrine sediments were deposited within an internally drained basin confined between the Atlas and Anti-Atlas Mountains (e.g. Görler *et al*. 1988; Fig. 9a). In contrast, its later history is dominated by erosion and began when the Draa river cut through the Anti-Atlas Mountains and the basin became externally drained (Fig. 9b–g). Stäblein (1988) suggested that the Draa river captured the Ouarzazate basin by regressive erosion. Alternatively, the piracy may have been induced when sediments overfilled the Ouarzazate basin and overtopped ridges of the Anti-Atlas, which allowed the southward drainage of streams from the basin via what is now the Draa river canyon (Fig. 3). In any case, the timing of the development of this superimposed drainage has yet to be defined,

Table 2. *Sample locations, descriptions, and terrestrial cosmogenic nuclide surface exposure data and ages*

Sample number	Surface	Latitude (°N)	Longitude (°W)	Altitude (m)	Lithology	Height/width/ breadth of sampled clast (cm)	Buried*	Weathering†	Sample thickness (cm)	^{10}Be atoms g^{-1} SiO_2 (10^5)	TCN age (no erosion)‖			TCN age (3 m Ma^{-1} erosion)‖		
											Age (ka)	Internal error (ka)	External error (ka)	Age (ka)	Internal error (ka)	External error (ka)
Maroc-4	Q1a	31.208	6.694	1590	Quartzite breccia	13/90/56	d	n	2.5	2.71 ± 0.11	21.8	0.9	2.2	23.1	1.0	2.5
Maroc-6	Q1a	31.209	6.695	1593	Unknown‡	17/15/6	s	n	6	18.40 ± 0.46	157.7	4.1	15.6	315.5	21.7	81.6
Maroc-7	Q1a	31.210	6.695	1595	Quartzite‡	11/7/4	s	s	4	23.65 ± 0.48	201.7	4.3	19.9	§	§	§
Maroc-8	Q1a	31.209	6.695	1594	Metaconglomerate‡	21/11/6	d	s	6	0.80 ± 0.07	6.6	0.6	0.8	6.7	0.6	0.8
Maroc-9	Q1a	31.209	6.695	1599	Red sandstone‡	15/11/8	s	n	8	24.27 ± 0.49	213.7	4.6	21.1	§	§	§
Maroc-10	Q1a	31.208	6.695	1592	Red sandstone‡	14/15/5	s	s	5	22.55 ± 0.46	193.1	4.1	19.0	706.2	183.2	842.1
Maroc-35	Q1b	31.227	6.724	1662	Quartzite	26/68/56	d	e	5	11.85 ± 0.31	94.1	2.5	9.2	127.3	4.9	17.6
Maroc-36	Q1b	31.226	6.724	1660	Quartzite	15/61/4	d	s	5	15.39 ± 0.50	123.9	4.2	12.4	194.3	11.5	34.0
Maroc-37	Q1b	31.226	6.724	1661	Quartzite	15/51/42	d	n	5	14.58 ± 0.32	117.1	2.6	11.3	177.0	6.6	28.3
Maroc-38	Q1b	31.227	6.723	1660	Quartzite	19/58/40	d	n	5	14.52 ± 0.36	117.2	3.0	11.4	177.2	7.5	28.6
Maroc-40	Q1b	31.229	6.724	1654	Quartzite	22/54/41	d	s	3	13.86 ± 0.35	109.2	2.8	10.6	158.5	6.4	24.1
Maroc-41	Q1b	31.229	6.724	1655	Quartzite	43/92/59	d	f	3	16.52 ± 0.41	131.2	3.4	12.8	215.1	10.4	39.3
Maroc-11	Q2	31.212	6.712	1603	Quartzite	26/46/40	d	s	4	19.40 ± 0.46	162.6	4.0	16.0	342.0	24.5	96.9
Maroc-13	Q2	31.228	6.713	1599	Rhyolite	18/48/34	d	n	4	20.38 ± 0.50	170.9	4.4	16.9	395.7	35.8	137.0
Maroc-14	Q2	31.228	6.714	1600	Siliceous volcanic rocks	20/49/40	d	n	4	20.84 ± 0.61	176.1	5.4	17.7	438.1	54.9	180.4
Maroc-15	Q2	31.227	6.714	1600	Rhyolite	35/71/37	m	n	3	34.24 ± 0.82	295.2	7.6	30.1	§	§	§
Maroc-16	Q2	31.225	6.713	1602	Siliceous volcanic rocks	18/65/36	m	n	3	15.53 ± 0.39	128.6	3.3	12.6	207.4	9.8	37.0
Maroc-17	Q2	31.226	6.714	1595	Quartzite	36/54/46	d	s	2	24.85 ± 0.63	208.8	5.6	20.9	§	§	§
Maroc-27	Q3a	31.271	6.680	1729	Rhyolite	37/114/120	d	n	3	11.42 ± 0.28	85.1	2.2	8.2	111.0	3.8	14.5
Maroc-29	Q3a	31.271	6.679	1735	Rhyolite	26/80/49	d	n	2	14.16 ± 0.34	105.2	2.6	10.2	149.9	5.6	22.1
Maroc-30	Q3a	31.272	6.679	1736	Rhyolite	47/106/75	d	f	3	12.73 ± 0.31	94.6	2.4	9.2	128.3	4.6	17.7
Maroc-31	Q3a	31.272	6.679	1737	Rhyolite	23/97/55	d	n	3	13.84 ± 0.35	102.9	2.7	10.0	145.0	5.7	21.1
Maroc-33	Q3a	31.270	6.679	1734	Rhyolite	39/87/53	d	n	3	12.65 ± 0.31	94.7	2.3	9.2	128.6	4.5	17.8
Maroc-34	Q3a	31.254	6.680	1738	Rhyolite	35/71/69	d	f	3	11.80 ± 0.29	87.6	2.2	8.5	115.5	3.9	15.3
Maroc-42	Q3b	31.199	6.691	1494	Rhyolite	15/58/34	d	s	2	11.41 ± 0.45	99.8	4.1	10.2	138.5	8.3	20.8
Maroc-43	Q3b	31.199	6.691	1494	Conglomerate	21/66/42	d	s	3	11.71 ± 0.37	104.3	3.4	10.3	147.7	7.2	22.1
Maroc-46	Q3b	31.199	6.692	1498	Rhyolite	20/61/44	d	n	2	9.97 ± 0.28	86.6	2.5	8.5	113.5	4.5	15.1
Maroc-47	Q3b	31.198	6.691	1496	Rhyolite	33/65/92	d	s	3	10.16 ± 0.35	88.8	3.2	8.9	117.5	5.8	16.2
Maroc-49	Q3b	31.195	6.689	1494	Sandstone	16/45/56	d	e	1	13.79 ± 0.33	120.5	3.0	11.7	185.2	7.8	30.6
Maroc-112	Q3c	31.166	6.802	1449	Psammite	26/42/70	d	n	5	98.11 ± 0.30	84.2	2.3	7.8	109.2	3.9	13.6
Maroc-113	Q3c	31.166	6.802	1449	Phyllite	20/30/75	d	n	5	10.83 ± 0.26	93.1	2.2	8.6	125.3	4.2	16.2
Maroc-115	Q3c	31.166	6.802	1448	Phyllite	22/25/55	d	s	6	10.26 ± 0.30	88.9	2.3	8.2	117.6	4.2	15.0
Maroc-116	Q3c	31.166	6.802	1450	Psammite	10/36/40	d	s	4	10.27 ± 0.24	87.4	2.2	8.0	114.9	3.9	14.4
Maroc-117	Q3c	31.165	6.803	1446	Psammite	18/25/52	m	n	4	10.38 ± 0.20	88.6	1.8	8.0	117.1	3.2	14.6
Maroc-20	Q4	31.203	6.689	1481	Rhyolite	60/151/81	d	n	2.5	4.11 ± 0.15	35.9	1.4	3.6	39.5	1.7	4.4
Maroc-21	Q4	31.202	6.688	1480	Rhyolite	70/165/125	d	n	2	2.60 ± 0.11	22.5	1.0	2.3	23.9	1.1	2.6
Maroc-22	Q4	31.201	6.688	1482	Rhyolite	63/120/80	d	n	2	0.97 ± 0.18	8.3	1.6	1.8	8.5	1.7	1.8
Maroc-23	Q4	31.201	6.688	1485	Gneiss	41/88/45	d	n	2	0.95 ± 0.06	8.2	0.5	0.9	8.4	0.6	1.0
Maroc-24	Q4	31.200	6.688	1482	Rhyolite	/88/52	m	f	5	0.80 ± 0.16	7.1	1.4	1.5	7.2	1.4	1.6
Maroc-25	Q4	31.200	6.689	1484	Rhyolite	66/147/84	m	n	3	1.21 ± 0.16	10.5	1.4	1.7	10.8	1.4	1.8
Maroc-26	Q4	31.200	6.688	1484	Siliceous volcanic rocks	46/76/66	m	n	2	1.27 ± 0.17	10.9	1.4	1.7	11.3	1.5	1.8
Maroc-50	Q6	31.231	6.695	1503	Rhyolite	23/38/66	d	n	2	2.17 ± 0.18	18.5	1.6	2.3	19.4	1.7	2.6
Maroc-51	Q6	31.231	6.695	1503	Rhyolite	30/30/50	d	n	3	0.06 ± 0.06	0.5	0.5	0.5	0.5	0.5	0.5

*d, deeply buried; m, moderate burial; s, slight burial.
†n, no noticeable weathering; s, slight weathering; f, fractures; e, exfoliation.
‡Cobble.
§Cannot calculate.
‖Internal error incorporates only analytical uncertainty, while external error incorporates both analytical and production rate uncertainty.

but it probably occurred during the late Pliocene or early Pleistocene, as there is little evidence of large cut–fill sequences within Tertiary red beds within the basin.

The extensive and deep incision developed throughout the Ouarzazate basin as the Draa river cut its way through the Anti-Atlas and essentially lowered the local base level has resulted in the succession of terraces we have described (Fig. 9b–g). The TCN ages for the terrace Q4 argue for climate and vegetation cover control of the fluvial behaviour at least for the last interglacial. Q4 TCN dates cluster between 7 and 11 ka (Table 2). These ages correspond to the abandonment and the start of incision of this terrace, now lying at 27 m above the active Madri channel. In the northern margin of the Sahara, south of the Atlas mountains of Algeria, after an arid glacial time, permanent lacustrine conditions prevailed during the early to mid-Holocene (from *c*. 11–10 to 5.7–3.3 ka; Gasse *et al*. 1987, 1990; Gasse 2000). Consistently, fluctuations in terrigenous supply to the continental margin off southern Morocco indicate an abrupt increase in humidity at 11.5–11 ka (Holz *et al*. 2007). This humid period correlates with the replacement of the Last Glacial Maximum (centred on *c*. 22 ka) cool grass–shrub steppe vegetation in north Africa (Lamb *et al*. 1989; Jolly *et al*. 1998; Elenga *et al*. 2000) by wooded biomes (temperate xerophytic wood or warm mixed forest in mountain catchments) that were present at elevations between 1200 and 2200 m a.s.l. by at least 6 ka (Reille 1979; Lamb *et al*. 1989, 1995; Salamani 1991, 1993; Jolly *et al*. 1998). Such a change in the vegetation cover suggest that vegetation-controlled slope stabilization in the beginning of the present interglacial reduced hillslope sediment supply to trunk streams, causing the end of fluvial aggradation in the Madri valley and, consequently, offering a mechanism for abandonment and incision of Q4.

Correlation with climatic cycles is not so straightforward for the older terraces (Q3 to Q1) because of uncertainties in the TCN ages (see Table 2). With regard to the Q3 surface, correcting for an erosion rate of 1 m Ma^{-1} places the most probable age of this terrace at 96–102 ka. If the same relationship to climate applies (i.e. incision during wet interglacial stages as for Q4), the abandonment of Q3 can be attributed to interglacial marine isotope stage 5e or the humid stadials of marine isotope stage 5 (specifically stage 5c).

Although direct palaeoclimate data for this epoch in Morocco

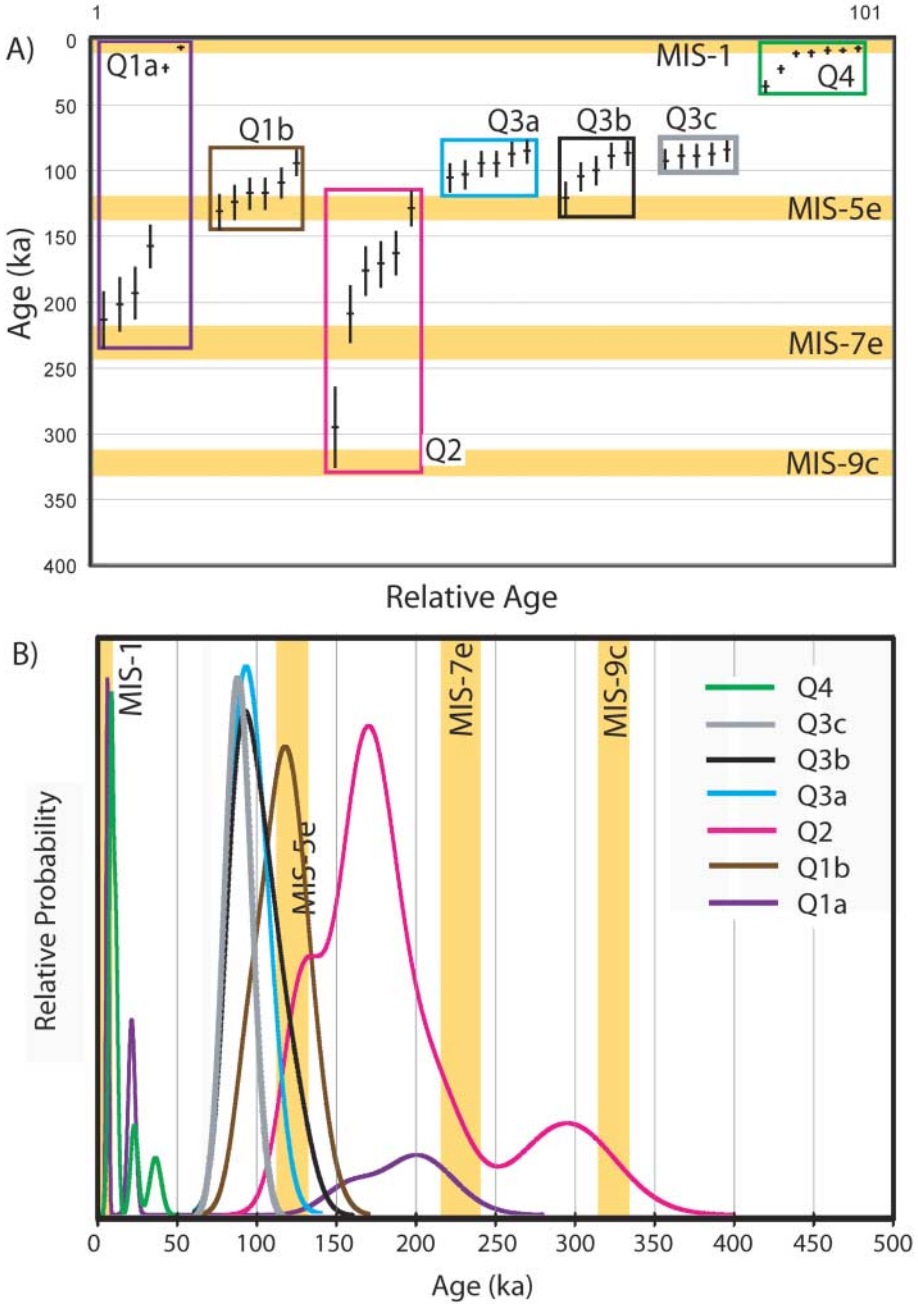

Fig. 8. TCN results plotted as (**a**) scatter graphs and (**b**) summed probability distributions for each surface. The duration of the interglacials MIS 1, 5e, 7e, and 9c (MIS, marine oxygen isotope stage) are based on the Devil's Hole $\delta^{18}O$ record (after Winograd *et al*. 1997).

are lacking, marine palaeoclimate records are available for the western Mediterranean (see, e.g. Cacho *et al*. 1999; Magri & Parra 2002; Hoogakker *et al*. 2004), but correlation with the terrestrial record across the Atlas Mountains is very tentative. Some of these issues have been discussed by Tzedakis (2007). However, previous studies on the Pleistocene fluvial behaviour of the Mediterranean region (e.g. Lewin *et al*. 1995; Fuller *et al*. 1998; Harvey *et al*. 1999*a*; Macklin *et al*. 2002; Santisteban & Schulte 2007; and references herein) provide important insights and have emphasized the sensitivity of fluvial systems to climate change, with sediment pulses in cold glacials or stadials and incision in warmer interglacials or interstadials. Climatic controls on alluvial fan and terrace development have long been recognized in other semi-arid settings, such as in the Basin and Range province and the Mojave Desert of the Western USA (Bull 1991; Harvey *et al*. 1999*b*). Moreover, Macklin *et al*. (2002) described a major river aggradation stage occurring at 109–111 ka (marine oxygen isotope stage 5d) in many Mediterranean catchments, a result that is broadly compatible with the age of aggradation that can be inferred for Q3.

We postulate that Q2 and Q1 correlate with the previous two interglacials. To our knowledge, independent data on humidity and vegetation cover in North Africa around these events are not available for either interglacial, but we may speculate that the same processes inferred for Q4 incision apply also for these cases.

Macklin *et al*. (2002) argued that, over the last 200 ka, fluvial aggradation phases generally occur during cool, dry glacials or

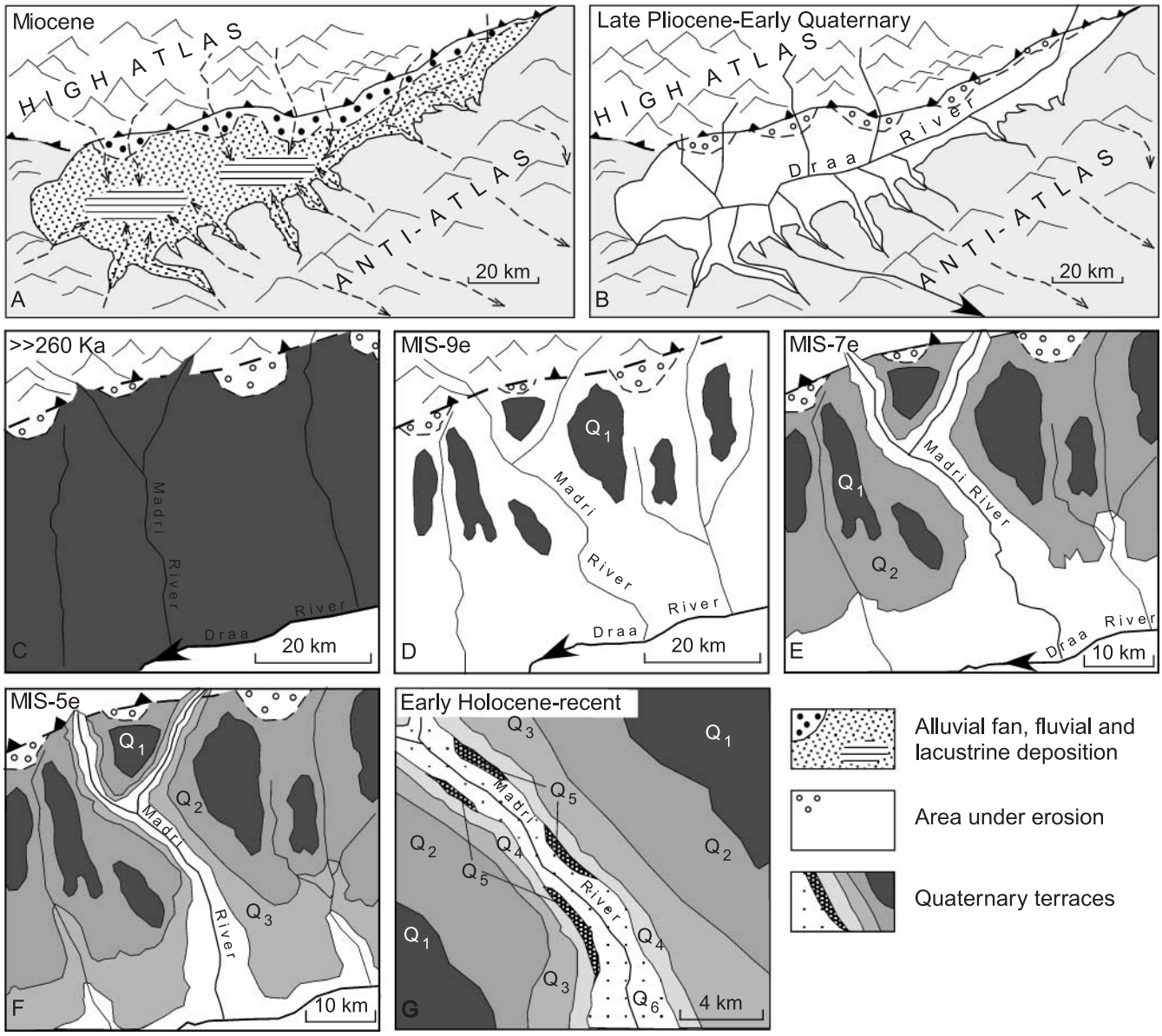

Fig. 9. Schematic diagrams showing the evolution of the Ouarzazate basin highlighting the formation of terraces along the Madri River.

stadials because catchment erosion is most active and associated rates of sediment supply are high. In consonance with what we can deduce for the Holocene, they suggested that this process is induced by changes in hydrology and vegetation cover: in periods of cool and dry climate, steppe vegetation replaces forest or wooded steppe biomes, the development of which occurs during warm and wet interglacials or interstadials. Conversely, Macklin *et al*. (2002) suggested that the inverse modification of vegetation cover at the transition between glacial and interglacial stages results in a decrease of the catchment erosion and associated sediment supply, in response to an increase in slope stability. Such processes together with an increase in humidity would be responsible for the incisions in the trunk streams that are documented around the Mediterranean for the interglacial stages. Climate change throughout glacial and interglacial cycles is complex and the relationship between precipitation changes may not be simple (see Cacho *et al*. 1999; McManus *et al*. 1999). Statements regarding precipitation changes between glacial and interglacials must therefore be regarded as somewhat tentative until independent proxies are available to quantify precipitation changes on Milankovitch and sub-Milankovitch time scales.

Glacial landforms have been described from the highest massifs of the High Atlas. These have been reviewed by Hughes *et al*. (2004, 2006). The timing of glaciation, however, is unknown, and thus this prevents any correlation of our fluvial aggradation–incision history with glaciation. The deduced snow-line for the coldest stages of the Pleistocene is >3300 m a.s.l. (see references given by Hughes *et al*. 2004, 2006). Hence, the extent of glaciation in the High Atlas was very limited, and it did not affect the Oued Madri catchment, most of which lies at an elevation below 3300 m a.s.l. Furthermore, the headwaters of our study area are about 10 km to the SSW of the glaciated catchments of the Central High Atlas (Mgoun massif) and would not have been directly affected by glacially controlled hydro-

logical changes. Glacial erosion processes, therefore, did not control sediment supply in the study area.

We can conclude that the TCN dates of the terraces within our study area provide evidence that abandonment of each terrace and fan occurred at intervals of *c*. 100 ka, that is, at glacial–interglacial time scales. Strong climatic control on fan development and sedimentation has been recognized for Quaternary fans and terraces in the foreland basins of other intracontinental mountain belts, notably the Gobi Altai Mountains (Owen *et al*. 1997). Our study provides one of the most comprehensive datasets for foreland basin landforms and it supports earlier speculation on the climatic control of landscape evolution in Morocco (e.g. Choubert 1965).

Surfaces Q1, Q2 and Q3 are tectonically deformed, with progressively more deformation on the older surfaces. The absence of notable deformation on surfaces Q4 and Q5 suggests that deformation progresses too slowly to deform Holocene surfaces to a noticeable extent, and that there has been no significant earthquake event during the last 10 ka that would have produced significant deformation. The newly dated surfaces now provide a framework for defining the magnitude of deformation throughout the Ouarzazate basin. In addition, the young ages on the deformed surface Q1b highlight the need to be careful when applying TCN surface exposure methods to deforming surfaces that may be progressively eroding.

The deformation of the fluvial terraces demonstrates that the transition from aggradation to erosion in the Ouarzazate basin occurred while thrust loading was still active along the High Atlas margin. The modification of the drainage pattern from internal to external and oscillations of the Quaternary climate are the dominant factors controlling erosion in the Ouarzazate basin at least during the past 300 ka. In addition, mantle-related uplift of the entire system of mountains and basins with respect to base level in the Late Cenozoic (Babault *et al*. 2008) provided additional potential for erosion to overtake subsidence and accumulation within the Ouarzazate basin.

Conclusions

The terrace and pediment incision in the active Ouarzazate foreland basin was primarily induced by a drop in base level as the main outlet channel of the basin, the Draa river, progressively cut through the Anti-Atlas Mountains to the south. Geomorphological analysis and TCN surface exposure dating show, however, that the development of Quaternary alluvial fans and terraces along the northern margin of the Ouarzazate basin is strongly controlled by climate oscillations on glacial–interglacial time scales. Surface abandonment ages for four terraces define their ages to the present and broadly last three interglacials. This suggests that incision occurs during interglacial times, when the region is wetter with hillslopes stabilized by wooded vegetation cover in mountainous catchments and streams are more pervasive, albeit still ephemeral. In contrast, during the more arid glacial times aggradation dominates, as increased hillslope erosion enhances sediment supply and the hydrological regime is less effective at transporting sediment. These data clearly demonstrate that knowledge of the character of climate change is essential to understand the nature of sediment transfer and landscape denudation in foreland basins. Surface exposure dating of abandoned fill-terraces suggests that rates of fluvial incision in this region range between 0.3 and 1.0 mm a^{-1} for the later part of the Quaternary. Furthermore, this study provides the first comprehensive TCN chronology for alluvial surfaces in Morocco and illustrates the problems associated with dating surfaces in this region that are significantly older than 100 ka.

We should like to thank J. Woodward, P. Hughes, D. Maddy and an anonymous reviewer for their very constructive and useful reviews of our manuscript. This work was supported by the Ministerio de Educación y Ciencia (Spain) projects CLG2005-25059 and CGL2006-07226, the Ministerio de Asuntos Exteriores AECI grant A/2921/05 and the CONSOLIDER-INGENIO 2010 project CDS2006-00041 (TOPOIBERIA). The TCN AMS analytical work was undertaken at the Lawrence Livermore National Laboratory (under DOE contract W-7405-ENG-48). M.L.A. benefited from a grant from the Salvador de Madariaga Program (MEC, Spain) during her sabbatical leave at the University of Cincinnati. She also thanks C. Dietsch and E. Ward for their hospitality during her stay. We thank C. Dietsch for his comments on an early version of this manuscript.

References

Akçar, N., Yavuz, V., Ivy-Ochs, S., Kubik, P.W., Vardar, M. & Schlüchter, C. 2007. Paleoglacial records from Kavron Valley, NE Turkey: Field and cosmogenic exposure dating evidence. *Quaternary International*, **164-165**, 170–183.

Allmetsat 2007. Climate of Ouarzazate, Morocco. World Wide Web Address: http://en.allmetsat.com/climate/morocco.php?code=60265.

Anders, M.D., Pederson, J.L. & Rittenour, T.M. *et al*. 2005. Pleistocene geomorphology and geochronology of eastern Grand Canyon; linkages of landscape components during climate changes. *Quaternary Science Reviews*, **24**, 2428–2448.

Anderson, R.S., Repka, J.L. & Dick, G.S. 1996. Explicit treatment of inheritance in dating depositional surfaces using *in situ* 10 Be and 26 Al. *Geology*, **24**, 47–51.

Arboleya, M.L., Teixell, A., Charroud, M. & Julivert, M. 2004. A structural transect through the High and Middle Atlas of Morocco. *Journal of African Earth Sciences*, **39**, 319–327.

Ayarza, P., Alvarez-Lobato, F., Teixell, A., Arboleya, M.L., Teson, E., Julivert, M. & Charroud, M. 2005. Crustal structure under the central High Atlas Mountains (Morocco) from geological and gravity data. *Tectonophysics*, **400**, 67–84.

Babault, J., Teixell, A., Arboleya, M.L. & Charroud, M. 2008. A Late Cenozoic age for long-wavelength surface uplift of the Atlas Mountains of Morocco. *Terra Nova*, **20**, 102–107, doi:10.1111/j.1365-3121.2008.00794.x.

Balco, G., Stone, J.O., Lifton, N.A. & Dunai, T.J. 2008. A complete and easily accessible means of calculating surface exposure ages or erosion rates from ^{10}Be and ^{26}Al measurements. *Quaternary Geochronology*, **3**, 174–195.

Beauchamp, W., Barazangi, M., Demnati, A. & El Alji, M. 1996. Intracontinental rifting and inversion: Missour Basin and Atlas Mountains, Morocco. *AAPG Bulletin*, **80**, 1459–1482.

Benn, D.I., Owen, L.A., Finkel, R.C. & Clemmens, S. 2006. Pleistocene Lake outburst floods and fan formation along the eastern Sierra Nevada: implications for the interpretation of intermontane lacustrine records. *Quaternary Science Reviews*, **25**, 2729–2748.

Bull, W.B. 1991. *Geomorphic Responses to Climatic Change*. Oxford University Press, New York.

Cacho, I., Grimalt, J.O., Pelejero, C., Canals, M., Sierro, F.J., Flores, J.A. & Shackleton, N.J. 1999. Dansgaard–Oeschger and Heinrich event imprints in Alboran Sea palaeotemperatures. *Palaeoceanography*, **14**, 698–705.

Choubert, G. 1965. Evolution de la connaissance du Quaternaire au Maroc. *Notes et Mémoires du Service Géologique du Maroc*, **25**, 9–27.

Choubert, G. & Faure-Muret, A. 1962. Evolution du domaine atlasique marocain depuis les temps paleozoïques. *In:* Choubert, G. & Faure-Muret, A. (eds) *Livre à la Mémoire du Professeur Paul Fallot*. Société Géologique de France, Mémoire hors série, **1**, 447–527.

Couvreur, G. 1973. Etagement de formes et néotectonique sur le versant sud du Haut Atlas. *Revue de Géomorphologie Dynamique*, **22**, 109–124.

DeCelles, P.G. & Giles, K.A. 1996. Foreland basin systems. *Basin Research*, **8**, 105–123.

Dresch, J. 1941. *Recherches sur l'évolution du relief dans le Massif Central du Grand Atlas, le Haouz et la Souss*. Arrault, Tours.

El Harfi, A., Lang, J., Salomon, J. & Chellai, E.H. 2001. Cenozoic sedimentary dynamics of the Ouarzazate foreland basin (Central High Atlas Mountains, Morocco). *International Journal of Earth Sciences*, **90**, 393–411.

Elenga, H., Peyron, O., Bonnefille, R., *et al*. 2000. Pollen-based biome reconstruction for southern Europe and Africa 18,000 yr BP. *Journal of Biogeography*, **27**, 621–634, doi:10.1046/j.1365-2699.2000.00430.x.

Flemings, P.B. & Jordan, T.E. 1989. A synthetic stratigraphic model of foreland basin development. *Journal of Geophysical Research*, **94**, 3851–3866.

Fraissinet, C., Zouine, E.M., Morel, J.L., Poisson, A., Andrieux, J. & Faure-Muret, A. 1988. Structural evolution of the southern and northern central High Atlas in Paleogene and Mio-Pliocene times. *In:* Jacobshagen, V.H. (ed.) *The Atlas System of Morocco*. Springer, New York, 272–291.

Frankel, K.L., Brantley, K.S., Dolan, J.F., *et al.* 2007a. Cosmogenic ^{10}Be and ^{36}Cl geochronology of offset alluvial fans along the northern Death Valley fault zone: Implications for transient strain in the eastern California shear zone. *Journal of Geophysical Research—Solid Earth*, **112**, B06407, doi:10.1029/2006JB004350.

Frankel, K.L., Dolan, J.F., Finkel, R.C., Owen, L.A. & Hoeft, J.S. 2007b. Spatial variations in slip rate along the Death Valley–Fish Lake Valley fault system determined from LiDAR topographic data and cosmogenic ^{10}Be geochronology. *Geophysical Research Letters*, **34**, LI8303, doi:10.1029/2007GL030549.

Frizon de Lamotte, D., Saint Bezar, B., Bracène, R. & Mercier, E. 2000. The two main steps of the Atlas building and geodynamics of the western Mediterranean. *Tectonics*, **19**, 740–761.

Fuller, I.C., Macklin, M.G., Lewin, J., Passmore, D.G. & Wintle, A.G. 1998. River response to high-frequency climate oscillations in Southern Europe over the past 200 k.y. *Geology*, **26**, 275–278.

Gasse, F. 2000. Hydrological changes in the African tropics since the last glacial maximum. *Quaternary Science Reviews*, **19**, 189–211.

Gasse, F., Fontes, J.C. & Plaziat, J.C. *et al.* 1987. Biological remains, geochemistry and stable isotopes for the reconstruction of environmental and hydrological changes in the Holocene lakes from North Sahara. *Palaeogeography, Palaeoclimatology, Palaeoecology*, **60**, 1–46.

Gasse, F., Tehet, R., Durand, A., Gilbert, E. & Fontes, J.-C. 1990. The arid–humid transition in the Sahara and the Sahel during the last deglaciation. *Nature*, **346**, 141–146.

Gile, L.H., Hawley, J.W. & Grossman, R.B. 1981. *Soils and geomorphology in the Basin and Range area of southern New Mexico; guidebook to the Desert Project*. New Mexico Bureau of Mines and Mineral Resources, Memoir, **39**.

Gomez, F., Beauchamp, W. & Barazangi, M. 2000. Role of the Atlas Mountains (northwest Africa) within the African–Eurasian plate-boundary zone. *Geology*, **28**, 775–778.

Görler, K., Helmdach, F.-F. & Gaemers, P. *et al.* 1988. The uplift of the central High Atlas as deduced from Neogene continental sediments of the Ouarzazate province, Morocco. *In:* Jacobshagen, V.H. (ed.) *The Atlas System of Morocco*. Springer, New York, 361–404.

Hancock, G.S., Anderson, R.S., Chadwick, O.A. & Finkel, R.C. 1999. Dating fluvial terraces with ^{10}Be and ^{26}Al profiles; application to the Wind River, Wyoming. *Geomorphology*, **27**, 41–60.

Harvey, A.M. & Wells, S.G. 1987. Response of Quaternary fluvial systems to differential epeirogenic uplift: Aguas and Feos River systems, south-east Spain. *Geology*, **15**, 689–693.

Harvey, A.M., Silva, P.G., Mather, A.E., Goy, J.L., Stokes, M. & Zazo, C. 1999a. The impact of Quaternary sea-level and climatic change on coastal alluvial fans in the Cabo de Gata Ranges, Southeast Spain. *Geomorphology*, **28**, 1–22.

Harvey, A.M., Wigand, P.E. & Wells, S.G. 1999b. Response of alluvial fan systems to the late Pleistocene to Holocene climatic transition; contrasts between the margins of pluvial lakes Lahontan and Mojave, Nevada and California, USA. *Catena*, **36**, 255–281.

Holz, C., Stuut, J.-B.W., Henrich, R. & Meggers, H. 2007. Variability in terrigenous sedimentation processes off Northwest Africa and its relation to climate changes; inferences from grain-size distributions of a Holocene marine sediment record. *Sedimentary Geology*, **202**, 499–508.

Hoogakker, B.A.A., Rothwell, R.G., Rohling, E.J., Paterne, M., Stow, D.A.V., Herrle, J.O. & Clayton, T. 2004. Aridity episodes during the last glacial cycle recorded in calcium carbonate records from the western Mediterranean Sea. *Marine Geology*, **211**, 21–43.

Hughes, P.D., Gibbard, P.L. & Woodward, J.C. 2004. Quaternary glaciation in the Atlas Mountains, North Africa. *In:* Ehlers, J. & Gibbard, P.L. (eds) *Quaternary Glaciation—Extent and Chronology. Volume 3: Asia, Latin America, Africa, Australia, Antarctica Elsevier, Amsterdam*. 255–260.

Hughes, P.D., Woodward, J.C. & Gibbard, P.L. 2006. Quaternary glacial history of the Mediterranean mountains. *Progress in Physical Geography*, **30**, 334–364, doi:10.1191/0309133306pp481ra.

Jacobshagen, V.H. 1988. Geodynamic evolution of the Atlas system, Morocco; an introduction. *In:* Jacobshagen, V.H. (ed.) *The Atlas System of Morocco*. Springer, New York, 3–9.

Jolly, D., Harrison, S.P., Damnati, B. & Bonnefille, R. 1998. Simulated climate and biomes of Africa during the late Quaternary; comparison with pollen and lake status data, Late Quaternary climates; data synthesis and model experiments. *Quaternary Science Reviews*, **17**, 629–657.

Kelly, M., Black, S. & Rowan, J.S. 2000. A calcrete-based U/Th chronology for landform evolution in the Sorbas basin, Southeast Spain. *Quaternary Science Reviews*, **19**, 995–1010.

Knippertz, P., Christoph, M. & Speth, P. 2003. Long-term precipitation variability in Morocco and the link to the large-scale circulation in recent and future climates. *Meteorology and Atmospheric Physics*, **83**, 67–88.

Kohl, C.P. & Nishiizumi, K. 1992. Chemical isolation of quartz for measurement of *in-situ*-produced cosmogenic nuclides. *Geochimica et Cosmochimica Acta*, **56**, 3583–3587.

Lal, D. 1991. Cosmic ray labeling of erosion surfaces; *in situ* nuclide production rates and erosion models. *Earth and Planetary Science Letters*, **104**, 424–439.

Lamb, H.F., Eicher, U. & Switsur, V.R. 1989. An 18,000-year record of vegetation, lake-level and climatic change from Tigalmamine, Middle Atlas, Morocco. *Journal of Biogeography*, **16**, 65–74.

Lamb, H.F., Gasse, F. & Benkaddour, A. *et al.* 1995. Relation between century-scale Holocene arid intervals in tropical and temperate zones. *Nature*, **373**, 134–137.

Laville, E. & Piqué, A. 1992. Jurassic penetrative deformation and Cenozoic uplift in the central High Atlas (Morocco); a tectonic model; structural and orogenic inversions. *Geologische Rundschau*, **81**, 157–170.

Le, K., Lee, J., Owen, L.A. & Finkel, R.C. 2007. Late Quaternary slip rates along the Sierra Nevada frontal fault zone, California: slip partitioning across the western margin of the Eastern California Shear Zone/Basin and Range Province. *Geological Society of America Bulletin*, **119**, 240–256.

Lewin, J., Macklin, M.G. & Woodward, J.C. (eds) 1995. *Mediterranean Quaternary River Environments*. Balkema, Rotterdam.

Macklin, M.G., Lewin, J. & Woodward, J.C. 1995. Quaternary fluvial systems in the Mediterranean Basin. *In:* Lewin, J., Macklin, M.G. & Woodward, J.C. (eds) *Mediterranean Quaternary River Environments*. Balkema, Rotterdam, 1–25.

Macklin, M.G., Fuller, I.C. & Lewin, J. *et al.* 2002. Correlation of fluvial sequences in the Mediterranean basin over the last 200 ka and their relationship to climate change. *Quaternary Science Reviews*, **21**, 1633–1641.

Magri, D. & Parra, I. 2002. Late Quaternary western Mediterranean pollen records and African wind. *Earth and Planetary Science Letters*, **200**, 401–408.

Mather, A.E. 2000. Adjustment of a drainage network to capture induced base-level change. *Geomorphology*, **34**, 271–289.

Matmon, A., Schwartz, D.P., Finkel, R., Clemmens, S. & Hanks, T. 2005. Dating offset fans along the Mojave section of the San Andreas fault using cosmogenic ^{26}Al and ^{10}Be. *Geological Society of America Bulletin*, **117**, 795–807.

Mattauer, M., Tapponier, P. & Proust, F. 1977. Sur les mécanismes de formation des chaînes intracontinentales. L'exemple des chaînes atlasiques du Maroc. *Bulletin de la Société Géologique de France*, **7**, 521–536.

McManus, J.F., Oppo, D.W. & Cullen, J.L. 1999. A 0.5 million-year record of millennial-scale climate variability in the North Atlantic. *Science*, **283**, 971–975.

Missenard, Y., Zeyen, H., Frizon de Lamotte, D., Leturmy, P., Petit, C., Sébrier, M. & Saddiqi, O. 2006. Crustal versus asthenospheric origin of relief of the Atlas Mountains of Morocco. *Journal of Geophysical Research*, **111**, B03401, doi:10.1029/2005JB003708.

Owen, L.A., Caffee, M.W., Bovard, K.R., Finkel, R.C. & Sharma, M.C. 2006. Terrestrial cosmogenic nuclide surface exposure dating of the oldest glacial successions in the Himalayan orogen: Ladakh Range, northern India. *Geological Society of America Bulletin*, **118**, 383–392.

Owen, L.A., Windley, B.F., Cunningham, W.D., Badamgarav, J. & Dorjnamjaa, D. 1997. Quaternary alluvial fans in the Gobi, southern Mongolia; evidence for neotectonics and climate change. *Journal of Quaternary Science*, **12**, 239–252.

Pigati, J.S. & Lifton, N.A. 2004. Geomagnetic effects on time-integrated cosmogenic nuclide production with emphasis on *in situ* ^{14}C and ^{10}Be. *Earth and Planetary Science Letters*, **226**, 193–205.

Reille, M. 1979. Analyse pollinique du lac de Sidi Bou Rhaba, littoral atlantique (Maroc). *Ecologia Mediterranea*, **4**, 61–65.

Rodgers, J. 1987. Chains of basement uplifts within cratons marginal to orogenic belts. *American Journal of Science*, **287**, 661–692.

Rose, J., Meng, X. & Watson, C. 1999. Palaeoclimate and palaeoenvironment responses in the western Mediterranean over the last 140,000 ka: evidence from Mallorca, Spain. *Journal of the Geological Society, London*, **156**, 435–448.

Salamani, M. 1991. Premières données palynologiques sur l'histoire Holocene du massif de l'Akfadou (Grande-Kabylie, Algérie). *Ecologia Mediterranea*, **17**, 145–159.

Salamani, M. 1993. Premières données paléophytogéographiques du Cèdre de l'Atlas (*Cedrus atlantica*) dans la région de grande Kabilie (NE Algérie). *Palynosciences*, **2**, 147–155.

Santisteban, J.I. & Schulte, L. 2007. Fluvial networks of the Iberian Peninsula: a chronological framework. *Quaternary Science Reviews*, **26**, 2738–2757.

Schaer, J.-P. 1987. Evolution and structure of the High Atlas of Morocco. *In:*

Schaer, J.-P. & Rodgers, J. (eds) *The Anatomy of Mountain Ranges*. Princeton University Press, Princeton, NJ, 107–127.

Schulte, L., Julià, R.J., Burjachs, F. & Hilgers, A. 2008. Middle Pleistocene to Holocene geochronology of the River Aguas terrace sequence (Iberian Peninsula): Fluvial response to Mediterranean environmental change. *Geomorphology*, **98**, 13–33.

Sébrier, M., Siame, L., Zouine, E.M., Winter, T., Missenard, Y. & Leturmy, P. 2006. Active tectonics in the Moroccan High Atlas. *Comptes Rendus Géosciences*, **338**, 65–79.

Sinclair, H.D., Coakley, B.J., Allen, P.A. & Watts, A.B. 1991. Simulation of foreland basin stratigraphy using a diffusion model of mountain belt uplift and erosion; an example from the Central Alps, Switzerland. *Tectonics*, **10**, 599–620.

Small, E.E., Anderson, R.S., Repka, J.L. & Finkel, R. 1997. Erosion rates of alpine bedrock summit surfaces deduced from *in situ* ^{10}Be and ^{26}Al. *Earth and Planetary Science Letters*, **150**, 413–425.

Stäblein, G. 1988. Geomorphological aspects of the Quaternary evolution of the Ourzazate basin, southern Morocco. *In:* Jacobshagen, V.H. (ed.) *The Atlas System of Morocco*. Springer, New York, 433–444.

Staiger, J., Gosse, J., Toracinta, R., Oglesby, B., Fastook, J. & Johnson, J.V. 2007. Atmospheric scaling of cosmogenic nuclide production: Climate effect. *Journal of Geophysical Research*, **112**, B02205, doi:10.1029/2005JB003811.

Stone, J.O. 2000. Air pressure and cosmogenic isotope production. *Journal of Geophysical Research*, **105**, 23753–23759.

Teixell, A., Arboleya, M.L., Julivert, M. & Charroud, M. 2003. Tectonic shortening and topography in the central High Atlas (Morocco). *Tectonics*, **22**, 1051, doi:10.1029/2002TC001460.

Teixell, A., Ayarza, P., Zeyen, H., Fernandez, M. & Arboleya, M.-L. 2005. Effects of mantle upwelling in a compressional setting: the Atlas Mountains of Morocco. *Terra Nova*, **17**, 456–461.

Tesón, E. & Teixell, A. 2008. Sequence of thrusting and syntectonic sedimentation in the eastern Sub-Atlas thrust belt (Dadès and Mgoun valleys, Morocco). *International Journal of Earth Sciences*, **97**, 103–113, doi:10.1007/s00531-006-0151-1.

Tzedakis, P.C. 2007. Seven ambiguities in the Mediterranean palaeoenvironmental narrative. *Quaternary Science Reviews*, **26**, 2042–2066.

Winograd, I.J., Landwehr, J.M., Ludwig, K.R., Coplen, T.B. & Riggs, A.C. 1997. Duration and structure of the past four interglaciations. *Quaternary Research*, **48**, 141–154.

Zehfuss, P.H., Bierman, P.R., Gillespie, A.R., Burke, R.M. & Caffee, M.W. 2001. Slip rates on the Fish Springs fault, Owens Valley, California, deduced from cosmogenic ^{10}Be and ^{26}Al and soil development on fan surfaces. *Geological Society of America Bulletin*, **113**, 241–255.

Zeyen, H., Ayarza, P., Fernàndez, M. & Rimi, A. 2005. Lithospheric structure under the western African–European plate boundary: A transect across the Atlas Mountains and the Gulf of Cadiz. *Tectonics*, **24**, TC2001, doi:10.1029/2004TC001639.

Ziegler, P.A., Cloetingh, S. & van Wees, J.-D. 1995. Dynamics of intra-plate compressional deformation; the Alpine Foreland and other examples. *Tectonophysics*, **252**, 7–59.

Received 24 October 2007; revised typescript accepted 1 May 2008.
Scientific editing by Jamie Woodward